Colloidal wettability probed with X-ray microscopy

Byung Mook Weon *, Ji San Lee, Ji Tae Kim, Jaeyeon Pyo, Jung Ho Je *

X-ray Imaging Center, Department of Materials Science and Engineering, Pohang University of Science and Technology, San 31, Pohang 790-784, Republic of Korea

ARTICLE INFO

ABSTRACT

Colloids (colloidal particles or nanoparticles) and their in-situ characterizations are important topics in colloid and interface science. In-situ visualization of colloids with X-ray microscopy is a growing frontier. Here, after a brief introduction on the method, we focus on its application for identifying nanoscale wettability of colloidal particles at fluid interfaces, which is a critical factor in colloidal self-assembly. We discuss a quantitative study on colloidal wettability with two microscopic methods: (i) X-ray microscopy by visualizing natural oil–water interfaces and (ii) confocal microscopy by visualizing fluorescently-labeled interfaces. Both methods show consistent estimation results in colloid–fluid interfacial tensions. This comparison strongly suggests a feasibility of X-ray microscopy as a promising in-situ protocol in colloid research, without fluorescent staining. Finally, we address a prospect of X-ray imaging for colloid and interface science.

© 2012 Elsevier Ltd. All rights reserved.

1. Introduction

X-ray photonics is undergoing a revolution in imaging capabilities with the use of ultrabright X-ray sources since the discovery of X-rays by Röntgen over a century ago [1]. X-ray imaging at nano- and microscale is of great interest for applications in physical and life sciences, including applied physics, materials science, biological imaging, environmental analysis, archeology, paleontology, and heritage restoration [2,3,4,5,6,7*,8*,9*,10,11*,12*], because it facilitates nondestructive, direct visualization of internal structures or elements.

In the recent years, there have been significant progress in the field of soft- and hard-X-ray microscopy, not only "technically", through the developments in source, optics, and imaging methodologies, but also "scientifically", through a wide range of applications [6,7*,8*,9*,10,11*,12*,13,14*,15,16,17,18,19,20,21,22,23,24*,25,26*,27*,28*,29,30,31*,32–34]. The associated wavelength range extends from a few nanometers to a small fraction of a nanometer, offering a potential to image objects at nanoscale spatial resolution [27*,28*,35*]. Furthermore, the large penetration depth of hard X-rays (wavelengths $\lambda = 0.01$–0.3 nm) allows relatively thick samples to be visible [28*], which is appropriate for in-situ visualization of colloids.

A number of powerful new X-ray imaging techniques are now available for research into colloidal morphologies (see the most recent comprehensive review [27*]). A series of technical hurdles have been overcome, allowing us to routinely image colloids with high coherence X-rays at the 10–50 nm length scale [27*,35*]. New techniques include X-ray ptychography, X-ray holography, quantitative phase X-ray microscopy, Talbot phase-contrast X-ray microscopy, and Fresnel-lens

X-ray microscopy [27*]. The methods are now competitive with optical microscopy (OM) [36], holographic microscopy (HM) [37,38*], video microscopy (VM) [39–41], confocal microscopy (CM) [42*,43,44], atomic force microscopy (AFM) [45–48], transmission electron microscopy (TEM) [49], and scanning electron microscopy (SEM) [50*] for imaging nanostructured materials.

In contrast to the existing techniques, hard X-ray microscopy has several advantages including less stringent sample preparation strategies than TEM and SEM, and the capability to study bulk morphologies unlike AFM and SEM [35*]. Without the need to microtome samples and stain them with heavy metals as in TEM, X-ray imaging can be performed for native specimens with reasonably large amounts of associated water [27*]. Furthermore, samples do not need to be held at low pressure and the X-ray techniques are sensitive to sub-surface structures unlike SEM [27*]. Specific advances with colloidal systems include the ability to measure the structure of colloids embedded inside other materials, the morphology of aerosols suspended in their natural gaseous state, and the strain in a single crystalline colloid [27*]. X-ray microscopy may be an alternative for characterizing properties of colloidal particles such as packing fraction [51], microrheology [52], and particle wettability [53].

Soft X-ray microscopy allows high-resolution imaging of several-micron-thick hydrated cells in a near-native state without chemical fixation, staining, or sectioning [28*]. This technique requires cryo-preservation of biological samples to avoid radiation damage [54,55] and utilizes the deep penetration ~10 μm using the natural differential absorption contrast between water and carbon (protein, lipids, etc.) provided by the water-window ($\lambda = 2.3$–4.4 nm or $E = 284$–540 eV) [56]. Soft X-ray microscopy within the water window can be used to study hydrated colloidal systems [57] if the systems are thinner than ~10 μm that corresponds to the depth of focus of

---

* Corresponding authors. Tel.: +82 54 279 2143; fax: +82 54 279 2992.
E-mail addresses: bmweon@hotmail.com (B.M. Weon), jhje@postech.ac.kr (J.H. Je).

soft X-rays [58•]. The highest spatial resolution of 10 nm was achieved in the soft X-ray range [59] and for hard X-rays, 20 nm resolution was recently reached [60].

In-situ visualization of colloids with X-ray microscopy is a growing frontier and the foreseeable future is positive [27••,35••]. Real-time monitoring of reaction kinetics involved in nanoparticle growth and transformation in liquid environments is crucial for understanding the complex chemical and physical events associated with nanophase evolution [61••]. It is very useful to directly visualize the nanometric and dynamic behaviors of colloids that are present inside or on fluids. After a brief introduction on the X-ray imaging method (particularly, the X-ray phase-contrast microscopy based on synchrotron hard X-rays), this review focuses on a promising application for the visualization and characterization of colloidal particles at fluid interfaces, showing a feasibility of X-ray imaging in colloidal wettability determination.

2. X-ray microscopy

In conventional X-ray radiography, contrast is obtained through the differences in the absorption cross-section (which is roughly proportional to the density) of the constituents of the object [7•]. The absorption-based imaging technique yields excellent results where highly absorbing structures such as bones are embedded in a medium of relatively weakly absorbing system (e.g., the surrounding tissue of the human body) [7•,8••]. The radiographic absorption imaging is an invaluable tool by clearly distinguishing between hard and soft structures in medical diagnostics and biomedical research [8••]. However, for biological samples, polymers, or fiber composites where the density difference is relatively weak, the use of the conventional X-ray radiography is limited due to the poor absorption contrast [7•]. This limitation is resolved by using a phase-sensitive imaging technique to improve the contrast, which is achievable at highly brilliant, coherent synchrotrons or micro-focus X-ray sources [2,3,4,5,6,7•,8••,9••,10,11•,12].

The phase-sensitive imaging technique requires a strong phase shift of X-rays through a sample and relies on the required spatial and temporal coherence lengths, described as $l_s = \lambda(\Delta\alpha/\alpha)^{-1}$ and $l_t = \lambda(\Delta E/E)^{-1}$, where λ is the wavelength, $\Delta\alpha/\alpha$ is the angular acceptance, and $\Delta E/E$ is the energy band pass of the crystal optics [7•,8••,9••,10,11•]. With typical values of $\Delta\alpha/\alpha \leq 10^{-4}$ and $\Delta E/E \leq 10^{-4}$, the coherence lengths range is in the order of $l_s \geq 1$ μm and $l_t \geq 1$ μm [7•,8••,9••,10,11•]. The temporal coherence length can be significantly improved by using a broad energy spectrum of $\Delta E/E \geq 10\%$ (corresponding to $l_t \sim 1$ nm) and the spatial coherence length of $l_s \geq 1$ μm is easily available from synchrotrons or micro-focus X-ray sources [7•].

The behavior of X-rays, as they travel through a sample, can be described using a complex index of refraction [8••]. For X-rays, the index of refraction (n) deviates slightly from unity; it can be written as $n = 1 - \delta - i\beta$, where β describes the absorption of X-rays and the phase-shift term δ incorporates the refractive effects [8••,12•]. At typical hard X-ray energies (>10 keV), the phase-shift terms (~10^{-7}) can be up to 1000 times greater than the absorption term (~10^{-10}) [8••,12•]. Thus, it is possible by adopting hard X-rays to effectively observe the phase contrast although the absorption contrast is undetectable [8••,12•]. X-rays passing through regions of different δ values make different phases and produce significant changes of wave fronts [8••]. These phase differences can be detected by using various phase-contrast techniques.

Fig. 1a illustrates the typical X-ray phase-contrast microscopy, based on the propagation of the X-ray wavefront in the near field (a small sample to detector distance, d), where d $\ll$ s²/λ (s is the structure size to resolve) [27••]. The experimental setup is relatively simple and the method is straightforward, consisting of source, sample, and detector. The source should provide partial coherent light and therefore the high brilliance of synchrotron radiation is very useful

[8••,12•]. For the sample fully illuminated, the edges of the structures can be enhanced by changing the distance between sample and detector (Fig. 1b). As a detector, a scintillator/mirror converts X-rays to visible lights and projects an image through an optical lens onto a CCD chip. Overall the in-line phase-contrast setup is very flexible, allowing real-time studies in many different types of environments such as pressure, stress, temperature, or magnetic fields on colloidal systems [27••].

In the in-line phase-contrast imaging, the detector is placed sufficiently far behind the sample (Fig. 1a). Here, the wavefront distortions generated by the sample produce interference fringes at the detector. At an appropriate sample-detector distance (d), these fringes contribute to edge enhancements in the image [8••]. For the X-ray phase-contrast imaging, the distance optimization is a critical factor in experiments: the increase in the sample-detector distance allows interference fringes to develop from the phase distortions in the X-ray beam wavefronts, improving the edge visibility (see the air–water interface in the lower panel of Fig. 1b). This phase-contrast-based technique is now a popular strategy in X-ray imaging to explore physical and biological sciences.

We have carried out studies on soft matter systems in a unique fashion by using hard X-ray microscopy [12•,13,14•,15–23,24••,25,26••]. A few recent studies for soft materials or colloids with X-ray (in-line) phase-contrast [20,21] and transmission X-ray (Zernike phase-contrast) microscopes (TXM) [24••] show great promise as a powerful tool of in-situ visualization for colloid and interface science. Fig. 1c–e exhibit useful examples of colloidal imaging with the in-line phase-contrast method (conducted at the 7B2 beamline at the Pohang Light Source): this method clearly visualizes dynamic behaviors during drying-mediated crystallization (Fig. 1c), a complicated colloid structure (Fig. 1d), and the cavities inside a colloidal packing (Fig. 1e). Interestingly X-rays can trigger dynamic changes in soft materials during X-ray irradiation [14•,17–19,23,24••]. For instance, hard X-rays can induce the changes in the surface tension of pure water droplets at the air/water interface [14•] or in the chemical bonds of polymers or colloidal particles [18,19,24••].

3. Colloidal wettability study

This part shows an application of the X-ray phase-contrast imaging for identifying nanoscale wettability of colloidal particles at fluid interfaces, which is a critical factor in colloidal self-assembly. We discuss a comparison between two microscopy methods: (i) X-ray microscopy by visualizing natural oil–water interfaces and (ii) confocal microscopy by visualizing fluorescently-labeled interfaces. The result in estimation of colloid–fluid interfacial tensions from visualization of wetting angles suggests a feasibility of X-ray microscopy as a promising in-situ protocol in colloidal wettability determination, without fluorescent staining.

3.1. Colloidal wettability

Colloidal particles or nanoparticles binding at fluid interfaces, particularly at oil–water interfaces, are widely studied because of scientific interest and potential applicability in nanotechnology and biotechnology [50•]. Colloidal particles, similar to surfactant molecules, can spontaneously accumulate at the interface between two immiscible fluids (liquid–gas or liquid–liquid) [62•]. The first realization of particle adsorption at interfaces is the pioneering works of Ramsden [63] and Pickering [64] a century ago. The strong binding of colloidal particles to fluid interfaces is evidenced by their ability to stabilize emulsions and foams [65•,66,67•,68•]. This irreversible adsorption can be a promising method to self-organize colloids or nanoparticles at interfaces in a well-defined manner [67•].

Colloidal self-assembly through suitable particle wettability is explained and predicted by the binding energy (ΔE) of a solid particle
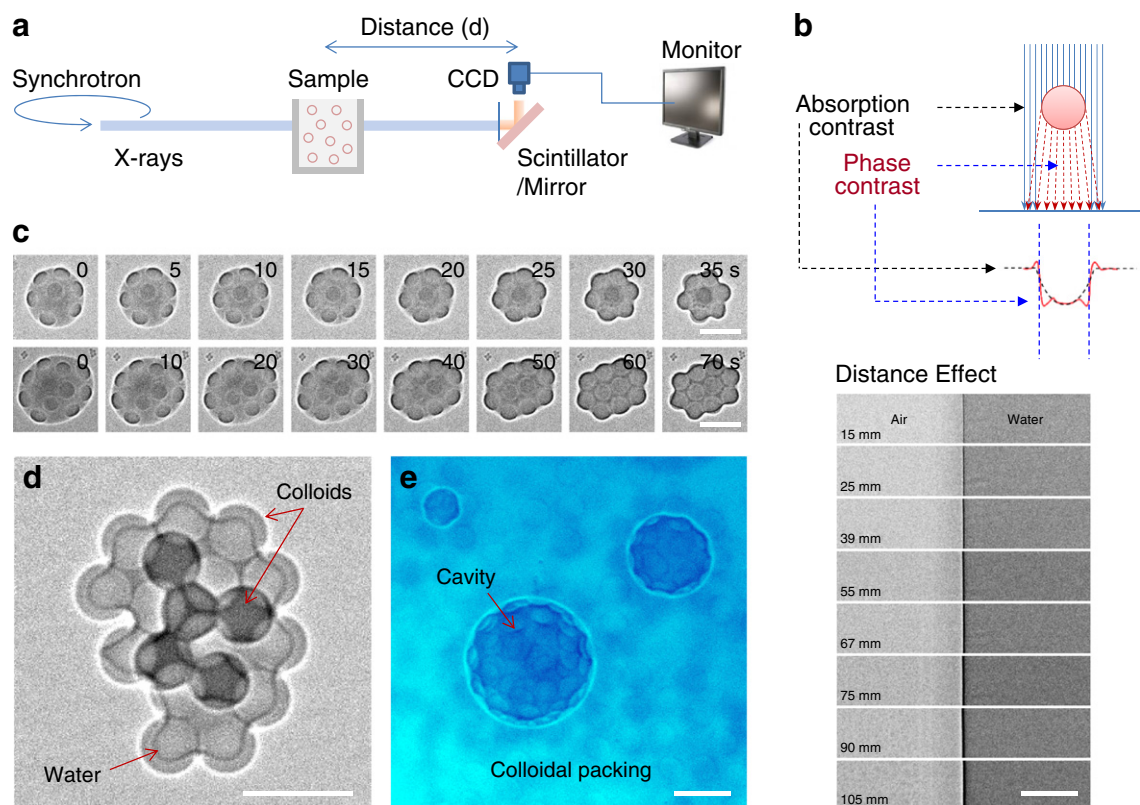
Fig. 1. Schematic illustration, principle, and example of X-ray microscopy. (a) Setup: the typical X-ray phase-contrast microscopy consists of source (X-rays from a synchrotron or a micro-focus source), sample, and detector (scintillator, mirror, CCD, and monitor) systems. This setup is very flexible, allowing real-time studies in many different types of environments such as pressure, stress, temperature, or magnetic fields on colloidal systems. (b) Principle: the X-ray wavefront distortions generated by the sample produce interference fringes at the detector (the upper panel). The increase in the sample-detector distance (d) allows interference fringes to develop from the phase distortions in the X-ray beam wavefronts, improving the edge visibility (see the air–water interface in the lower panel). (c)–(e) Example: the X-ray phase-contrast imaging (conducted at the 7B2 beamline at the Pohang Light Source) clearly visualizes dynamic behaviors during drying-mediated crystallization (c), a complicated colloid structure (d), and the cavities inside a colloidal packing (e). Scale bars: 100 μm.

of radius (r) at the interface between immiscible fluids with fluid–fluid interfacial tension (e.g., γ_{OW} for oil–water) as: $\Delta E = -\pi r^2 \gamma_{OW}(1 - \cos\theta)^2$ [69], excluding line-tension or image-charge contributions [50*,70]. Here a key parameter to control the adsorption of solid particles at fluid interfaces is the particle three-phase contact angle (θ) for a given particle size and interfacial tension. The contact angle (through water) of colloids at oil–water interfaces depends on the interfacial tensions at the particle–water, γ_{PW}, particle–oil, γ_{PO}, and oil–water, γ_{OW}, interfaces according to Young's equation: $\cos\theta = (\gamma_{PO} - \gamma_{PW})/\gamma_{OW}$ [62*,63,64,65*,66,67*]. Generally, hydrophilic ($0° < \theta < 90°$) particles are preferentially wet by water ($\gamma_{PO} > \gamma_{PW}$) and thus oil-in-water emulsions are preferred, while hydrophobic ($90° < \theta < 180°$) particles are wet by oil ($\gamma_{PO} < \gamma_{PW}$) and water-in-oil emulsions are preferred [62*,66].

In practice, θ is difficult to measure accurately for colloidal particles, and it may differ substantially from the contact angle measured in a macroscopic system of the same materials [67*]. The current technologies, for instance, cryo-scanning electron microscopy (cryo-SEM) [50*] and atomic force microscopy-added gel-trapping technique (AFM-GTT) [71], usually adopt complicated sample preparations, which may reduce data precision. Colloidal particles adsorbing at a planer undeformed oil–water interface are a challenging system, because the particle surface and the interface are optically unclear [72]. As illustrated in Fig. 2, particle-stabilized emulsion droplets are typically visualized by fluorescently-labeled particles with confocal microscopy. Here the unlabeled oil–water interface is invisible. To measure the particle contact angle, an in-situ differentiation between the particle surface and the fluid interface with nanoscale resolution is required.

An important challenge for colloidal particles is to measure the particle contact angle of polymethylmethacrylate (PMMA) colloids that have been studied as a model hard-sphere system for three decades [73–75]. To realize uniform dispersion of colloids in a liquid medium such as decalin, steric stabilization is usually adopted by chemically grafting polymer "brushes" onto the surface of colloidal particles; the brushes provide elastic repulsion when two particles approach so closely that their brushes are compressed [75]. The PMMA colloids suspended in decalin are usually stabilized by poly(12-hydroxystearic acid) (PHSA) chains. Here the PHSA chains are expected to change the interfacial tension of PMMA from that of pure PMMA. However the interfacial tensions associated with the PHSA-grafted PMMA colloids at a decalin–water interface are not known [76].

For the PHSA-coating PMMA particles at the decalin–water interface, we introduce in-situ visualization methods to measure the colloidal wettability (θ) using in-situ X-ray microscopy for natural oil–water interfaces and confocal microscopy for fluorescently-labeled interfaces. Using the θ values, we estimate the interfacial tensions of γ_{PA}, γ_{PO}, and γ_{PW}, based on Fowkes approximation, which is typically used to estimate interfacial tensions between polar water and apolar hydrocarbons (or solids) [77,78*]. Both in-situ visualization methods, using X-ray and confocal microscopies, show consistent results in the interfacial tension estimation, suggesting feasibility with precision and simplicity for the wettability determination of colloidal particles.

As model colloids, we use ~2-μm-diameter, monodispersed PMMA spheres with a thin (10–20 nm) grafted layer of PHSA (PHSA-g-PMMA), synthesized by Andrew Schofield [79]. The particles have diameters of 2.2 μm for X-ray imaging and 2.0 μm for confocal imaging with ~5%

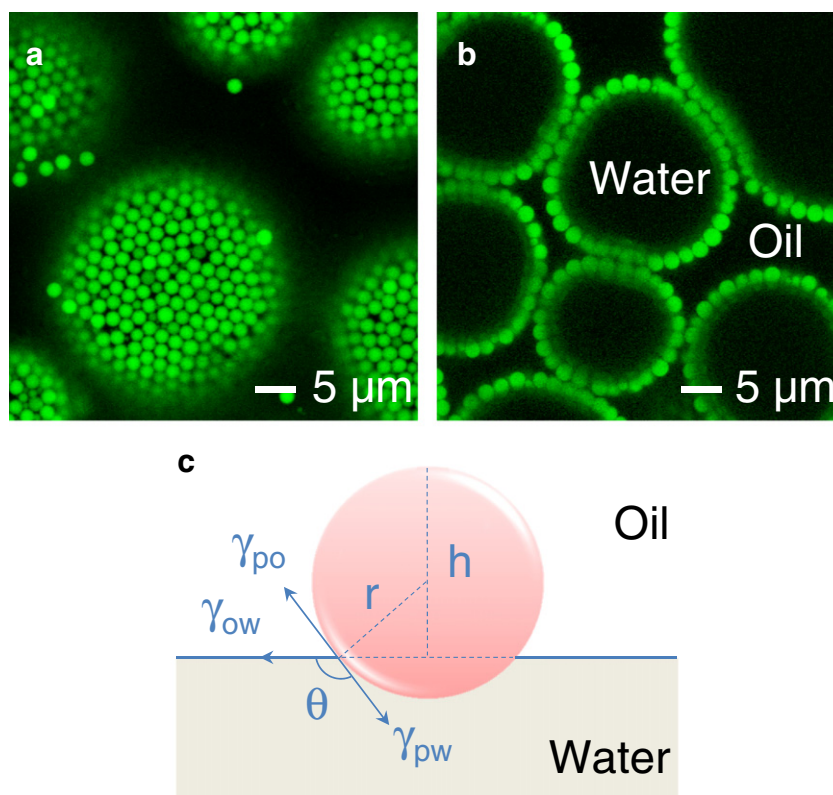**Fig. 2.** Colloids on oil–water interfaces. (a) and (b) Confocal imaging for particle-stabilized emulsions droplets, where ~2-μm-diameter, fluorescently-labeled PHSA-g-PMMA colloids are visible between decalin and water but the unlabeled (natural) decalin–water interfaces are invisible. The particle three-phase contact angle (θ) is inaccessible with this imaging. (c) Thermodynamic geometry of a single colloid adsorbing at an oil–water interface. The contact angle (through water) depends on the interfacial tensions at the particle–water, γ_{PW}, particle–oil, γ_{PO}, and oil–water, γ_{OW}, interfaces according to Young's equation: $\cos\theta = (\gamma_{PO} - \gamma_{PW})/\gamma_{OW}$, excluding line-tension and image-charge contributions. The contact angle and the particle radius (r) determine the immersion depth into oil, $h = r(1 - \cos\theta)$. The key quantities of θ, γ_{PO}, and γ_{PW} are typically unknown for colloidal particles.

polydispersity in size (determined by dynamic light scattering; ALV 5000, 532 nm laser, 90° scattering angle). The PHSA-g-PMMA particles (density $\rho_{PMMA} = 1.19$ g/cm^3; refractive index $n_{PMMA} = 1.49$) are suspended in decalin (decahydronaphthalene; mixture of *cis*- and *trans*-decalin; $\rho_{dec} = 0.897$ g/cm^3 and $n_{dec} = 1.48$) [25,80,81].

3.2. X-ray microscopy of colloids

To directly obtain the θ value from an oil–water interface, we applied the full-field transmission X-ray microscopy (TXM), as illustrated in Fig. 3a, at a photon energy of 8 keV on the 32-ID beamline of the Advanced Photon Source at the Argonne National Laboratory [24••]. This approach offered the simplest way to visualize colloidal particles that irreversibly adsorb and bind at a natural oil–water interface (here 'natural' means no addition of fluorescent dyes or surfactants). For X-ray imaging, we made stable oil–water emulsion drops using the colloids, decalin, and ultrapure water (18 MΩ, Millipore) (see Fig. 2), and then insert the drops in decalin within a 10-μm-thick microcapillary tube. In-situ X-ray imaging could clearly visualize the natural oil–water interface and the colloid surface, as illustrated in Fig. 3b. To reduce possible sample deterioration by chain scission with a long (>30 s) X-ray exposure [24••], we adopted a very short (~1 ms) exposure to take images. As a result, image contrast was slightly decreased but sufficient to differentiate the colloid surface from the oil–water interface. The immersion depth of the particle in oil is given as: $h = r(1 - \cos\theta)$ by the geometry in Fig. 2c. The geometric relation is used to obtain the particle contact angle at the natural oil–water interface as: $\theta = a\cos(1 - h/r)$. The contact angle is $\theta = 167.4° \pm 12.0°$, coming from the measured values for h and $2r$ (Fig. 3b, the inset), where the error bar means a standard deviation from ten data.

3.3. Confocal microscopy of colloids

To identify the oil–water interface with confocal imaging, we used a labeled water (with rhodamine-B of ~0.01 wt.%) and fluorescently-labeled colloids of ~0.001% volume fraction suspended in non-labeled decalin (as "oil" phase). The labeled interface was placed between two parallel cover glasses (VWR, 22×30 mm^2) separated by ~1 mm to reduce wall effects. The colloidal particles instantly bound to the oil–water interface. The adsorbed single particle and the interface were visualized in different colors using a confocal microscope (Leica TCS SP5) with oil immersion objective (100×1.4 numerical aperture), Ar+ laser excitation (488 nm excitation), and multichannel detector (TD488/543/633; PMT1, 500–570 nm for PHSA-g-PMMA and PMT2, 580–600 nm for water). The best image size was 512×512 pixels (14.83×14.83 μm^2). To distinguish the particle from the interface, we adopt different dyes for the particle and the water phase (Fig. 4a), allowing us to directly determine the particle contact angle for the labeled water–oil interface. The measured contact angle is $\theta = 170° \pm 10°$ from five data.

3.4. Estimation of interfacial tensions

The particle contact angles, obtained by in-situ visualization methods with X-ray and confocal microscopies, are essential to estimate the colloid–fluid interfacial tensions. Notably, the contact angle of the PHSA-g-PMMA colloids in decalin at the decalin–air interface is almost zero ($\psi = 0$) or $\cos\psi = (\gamma_{PA} - \gamma_{PO})/\gamma_{OA} = 1$ [81], because no adsorption at the interface is found with X-ray imaging (data not shown). From Young's equations for the particle contact angles (θ and ψ at oil–water and oil–air interfaces, respectively), we
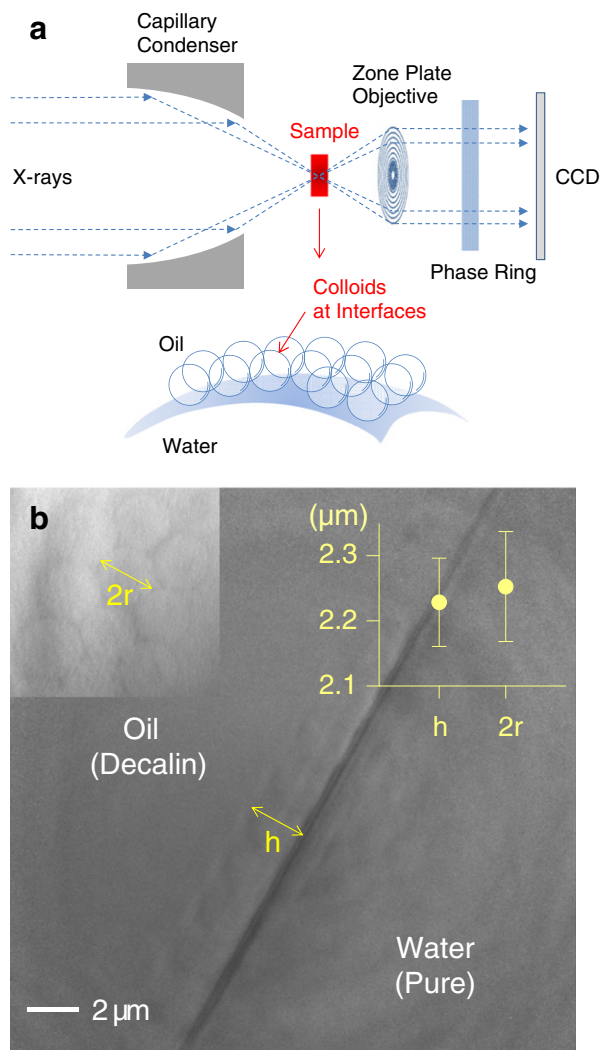
Fig. 3. X-ray imaging of colloids at interfaces. (a) Schematic illustration of the full-field transmission X-ray microscopy (conducted at the 32-ID beamline at the Advanced Photon Source) [24]. (b) The method was used to directly visualize a monolayer of colloids on an emulsion droplet. This is the simplest in-situ visualization method for the contact angle from a natural oil–water interface. The image size was 512×512 pixels (22.11×22.11 μm^2) and its resolution was 43 nm/pixel. The particle diameter ($2r$, the left inset, from the top-view imaging) and the immersion depth into oil (h, from the side-view imaging) were directly measured (the right inset) and in turn the particle contact angle, $\theta = \mathrm{acos}(1 - h/r)$, was obtained as $\theta = 167.4° \pm 12.0°$ (the error bar means a standard deviation from ten data).
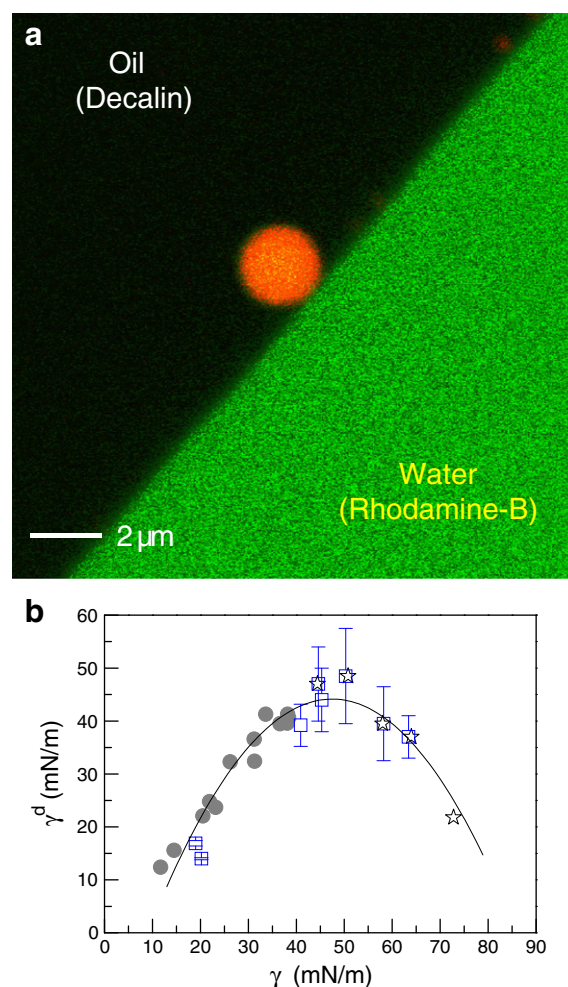

Fig. 4. Confocal imaging of colloids at interfaces. (a) High-resolution confocal microscopy (Leica TCS SP5) was used to directly visualize a single colloid at a planer undeformed, fluorescently-labeled (rhodamine-B) water–decalin interface, between two parallel cover glasses. This is the simplest in-situ visualization method for the contact angle measurement from a labeled water–oil interface. The image size was 512×512 pixels (14.83×14.83 μm^2) and its resolution was 29 nm/pixel. The labeling of water by rhodamine-B significantly changes the oil–water interfacial tension, which is used to estimate the colloid–fluid interfacial tensions. The contact angle was measured as $\theta = 170° \pm 10°$ from five data. (b) Fowkes approach for estimating the interfacial tension between polar water and apolar colloids (or hydrocarbons), based on the dispersion force. A general relation between the dispersion force (γ^d) and the interfacial tension (γ) is found as $\gamma^d = -23.0207 + 2.8297\gamma - 0.0298\gamma^2$ (the solid line), estimated from literature for polar liquids (the squares [77] and the stars [78•]) and for polymeric solids (the circles) [78•] with a high coefficient of determination as $R^2 = 0.9175$.

derive a relation: $\gamma_{OA} + \gamma_{OW}\cos\theta = -(\gamma_{PW} - \gamma_{PA})$. Here the fluid–fluid interfacial tensions (γ_{OA} and γ_{OW}) are well known and the particle contact angles (θ and ψ) can be measured with the in-situ methods, whereas the colloid–fluid interfacial tensions (γ_{PW} and γ_{PA}) are unknown.

To determine the quantity of ($\gamma_{PW} - \gamma_{PA}$), we adopt the simplest theoretical approach, which was developed by Fowkes to determine the interfacial tensions between polar water (W) and apolar solids (P) [77,78•]. According to the so-called *Fowkes equation*, the interfacial tension for a particle–water system by London dispersion forces for particle (γ_P^d) and for water (γ_W^d) can be given as: $\gamma_{PW} = \gamma_{PA} + \gamma_{WA} - 2(\gamma_P^d \gamma_W^d)^{1/2}$. Here the water–air interfacial tension is $\gamma_{WA} = 72.8$ mN/m (at 20 °C), the particle dispersion force component is $\gamma_P^d = \gamma_{PA}$ (assumed for apolar solids), and the water dispersion force component is $\gamma_W^d = 21.8$ mN/m [77,78•]. The oil–water interfacial tension can be precisely estimated from the Fowkes equation by replacing particle (P) with oil (O). For example, $\gamma_{OW} = 51.8$ mN/m is estimated for the decalin–water

interface using the decalin–air interfacial tension $\gamma_{OA} = 31.0$ mN/m [25,81]. By combining the Young and the Fowkes equations, we obtain the following expression of the particle–air interfacial tension as $\gamma_{PA} = (\gamma_{OW}\cos\theta + \gamma_{OA} + \gamma_{WA})^2/(4\gamma_W^d)$, called the Fowkes approximation. Here the values of γ_{OW}, γ_{OA}, γ_{WA}, and γ_W^d are known, and the value of $\cos\theta$ can be determined by the visualization methods. As a result, the particle–air interfacial tension is finally measured as $\gamma_{PA} \approx 32.5$ mN/m, resulting in the particle–oil and particle–water interfacial tensions as $\gamma_{PO} \approx 1.5$ mN/m and $\gamma_{PW} \approx 52.1$ mN/m from the Young equations for θ and ψ using X-ray imaging.

In confocal imaging, the estimation approach is identical with X-ray imaging, except for the fluorescently-labeled water (V): one needs to replace W with V. The labeling of water by rhodamine-B significantly changes the oil–water interfacial tension as $\gamma_{OV} = 49.0$ mN/m [82], which modifies the dispersion force component of the labeled water, γ_V^d. We note that the dispersion force component has a quadratic relation with the interfacial tension component:

$\gamma^d = -23.0207 + 2.8297\gamma - 0.0298\gamma^2$ (estimated from literature [77,78[*]]; the coefficient of determination is high as $R^2 = 0.9175$; Fig. 4b). This relation can be used to estimate the dispersion force component of the rhodamine-labeled water as $\gamma_V^d = 44.1$ mN/m. This result leads to the interfacial tensions $\gamma_{OV} = 6.1$ mN/m for the labeled water–oil interface and finally $\gamma_{PA} \approx 31.1$ mN/m, $\gamma_{PO} \approx 0.1$ mN/m, and $\gamma_{PV} \approx 6.0$ mN/m for the colloid–fluid interfaces, based on the particle contact angle ($\approx 170°$) using confocal imaging.

Most importantly, both the methods, based on in-situ X-ray or confocal imaging, show consistent estimates of the colloid–fluid interfacial tensions of γ_{PA} and γ_{PO}, regardless of the labeling of water. This result thus suggests that the X-ray imaging methods can be feasible protocols in the colloidal wettability determination.

The current state-of-the-art techniques, for instance, cryo-SEM and AFM-GTT, show high accuracy but no information about data precision. For 2-μm-diameter PMMA colloids at n-decane/water interfaces [50[*]], the Fowkes equation suggests the n-decane/water interface to have $\gamma_{OW} = 51.0$ mN/m from $\gamma_{OA} = 23.9$ mN/m [77]. From the Fowkes approximation, we estimate the particle contact angle as $\theta \approx 148.3° - 151.0°$, based on $\gamma_{PA} \approx 31.1 - 32.5$ mN/m (our result). We believe that this estimate (148.3°–151.0°) is more precise than those by AFM-GTT (157.4° ± 5.3°) and cryo-SEM (129.8° ± 11.8°) [50[*]]. It is well known that a spreading solvent in AFM-GTT makes the particle more hydrophobic [83]. On the other hand, the deposition process in cryo-SEM [50[*]] may make the particle more hydrophilic by gravity effect because the gravity force (mg) is almost twice than the thermal force ($k_B T/r$) for 2-μm-diameter PMMA particles [84] (where m is the buoyant weight, g is the gravity acceleration, k_B is the Boltzmann constant, and T is the temperature). In our methods, the gravity effect is minimized by using particle-stabilized emulsions and by inducing the particle adsorption regardless of the gravity.

This application study shows a feasibility of X-ray microscopy for visualization and characterization of colloidal particles. Nanoscale wettability of colloidal particles at fluid interfaces is an essential factor in colloidal self-assembly [85,86]. The X-ray imaging methods for colloids deserve further studies in different colloid and fluid systems.

4. Outlook

The current state of the art methods for direct visualization of colloidal particles with X-ray microscopy typically provide the practical resolution in the range of 10–50 nm [27[**],35[**]]. Many scientists are racing to harness billion-dollar synchrotron facilities to generate and use ever-smaller hard X-ray microbeams and nanobeams (5 to 100 keV) [35[**]]. This race toward smaller X-ray beams is driven by three factors: (i) the fundamental interactions of X-rays with matter that allow for powerful characterization methods; (ii) the inhomogeneous nature of natural and human-made materials; and (iii) the emergence of ultrabrilliant synchrotron sources and efficient X-ray focusing optics. X-ray nanobeams as small as 7 nm are now available, and the practical limit for hard X-ray beam size, the limit to trace-element sensitivity, and the ultimate limitations associated with near-atomic structure determinations are the subject of ongoing research [35[**]]. The achievable spot size for 10 keV X-rays has been revolutionized by major advances in precision fabrication of mirrors and zone plates and by new concepts [35[**]]. As the X-ray beam spatial resolution improves, the kind of science that is possible has begun to overlap the domain of electron microscopy methods, including electron holography, transmission electron microscopy, and quantitative scanning electron microscopy [35[**]]. The main advantage of X-rays over more readily available electron methods is their ability to probe samples buried in hostile environments, underwater, and/or through layered structures, and the tremendous quantitative sensitivity of X-rays to trace elements and structures [27[**]]. When combined, the emerging suite of electron and X-ray structural probes may

enable us to characterize colloidal particles over all hierarchical length scales ranging from atomic to macroscopic [35[**]].

Three-dimensional (3D) imaging can be achieved through sequential two-dimensional (2D) imaging of rotated samples, followed by computed tomography image-reconstruction techniques, and can be performed in several minutes [28[*]]. During recent years, 3D X-ray imaging methods have advanced tremendously [87–90]. The high penetration power of X-rays provides the ability to see inside macroscopic objects in a non-invasive way [87,88]. The high-resolution X-ray micro-tomography techniques at brilliant synchrotron sources may allow 3D imaging of colloidal samples at resolutions better than 100 nm. The possibility for 3D visualization of colloids with X-rays may open up new research topics on colloids and interfaces.

Consequently, to advance our understanding of colloidal particles, X-ray microscopy is highly competitive with other microscopies in visualizing colloidal particles [91[*],92[*],93–102].

References[*],[**]

[1] Röntgen WC. On a new kind of rays. Nature 1896;53:274-6.
[2] Davis TJ, Gao D, Gureyev TE, Stevenson AW, Wilkins SW. Phase-contrast imaging of weakly absorbing materials using hard X-rays. Nature 1995;373:595-8.
[3] Snigirev A, Snigireva I, Kohn V, Kuznetsov S, Schelokov I. On the possibilities of x-ray phase contrast microimaging by coherent high-energy synchrotron radiation. Rev Sci Instrum 1995;66:5486-92.
[4] Wilkins SW, Gureyev TE, Gao D, Pogany A, Stevenson AW. Phase-contrast imaging using polychromatic hard X-rays. Nature 1996;384:335-8.
[5] Momose A, Takeda T, Itai Y, Hirano K. Phase-contrast X-ray computed tomography for observing biological soft tissues. Nat Med 1996;2:473-5.
[6] Tsai WL, Hsu PC, Hwu Y, Chen CH, Chang LW, Je JH, Lin HM, Groso A, Margaritondo G. Electrochemistry: building on bubbles in metal electrodeposition. Nature 2002;417:139.
[7] Pfeiffer F, Weitkamp T, Bunk O, David C. Phase retrieval and differential phase-contrast imaging with low-brilliance X-ray sources. Nat Phys 2006;2: 258-61.
[8] Fitzgerald R. Phase-sensitive x-ray imaging. Phys Today 2000;53:23-6.
[9] Hwu Y, Tsai WL, Groso A, Margaritondo G, Je JH. Coherence-enhanced synchrotron radiology: simple theory and practical applications. J Phys D: Appl Phys 2002;35:R105-20.
[10] Lewis RA. Medical phase contrast x-ray imaging: current status and future prospect. Phys Med Biol 2004;49:3573-83.
[11] Momose A. Recent advances in X-ray phase imaging. Jpn J Appl Phys 2005;44: 6355-67.
[12] Weon BM, Je JH, Hwu Y, Margaritondo G. Phase contrast X-ray imaging. Int J Nanotechnol 2006;3:280-97.
[13] Weon BM, Je JH, Hwu Y, Margaritondo G. Stable freestanding thin films of pure water. Appl Phys Lett 2008;92:104101.
[14] Weon BM, Je JH, Hwu Y, Margaritondo G. Decreased surface tension of water by hard-X-ray irradiation. Phys Rev Lett 2008;100:217403.
[15] Weon BM, Je JH, Hwu Y, Margaritondo G. A coherent synchrotron X-ray microradiology investigation of bubble and droplet coalescence. J Synchrotron Radiat 2008;15:660-2.
[16] Weon BM, Je JH. Ionization-induced surface tension reduction of water droplets. Appl Phys Lett 2008;93:244105.
[17] Kwon YB, Weon BM, Won KH, Je JH, Hwu Y, Margaritondo G. X-ray-induced changes in wettability. Langmuir 2009;25:1927-9.
[18] Weon BM, Chang S, Yeom J, Hahn SK, Je JH, Hwu Y, Margaritondo G. X-ray ablation of hyaluronan hydrogels: fabrication of three-dimensional microchannel networks. J Appl Phys 2009;106:053518.
[19] Weon BM, Kwon YB, Won KH, Yoo J, Je JH, Li M, Hahn JH. Ablation and deposition of poly(dimethylsiloxane) with X-rays. Chemphyschem 2010;11:115-8.

---

[*] Of special interest.
[**] Of outstanding interest.

[20] Weon BM, Je JH. Capillary force repels coffee-ring effect. Phys Rev E 2010;82: 015305.
[21] Weon BM, Je JH, Gremaud G. Hard X-ray imaging for landslide research. J Synchrotron Radiat 2010;17:817-20.
[22] Weon BM, Je JH, Poulard C. Convection-enhanced water evaporation. AIP Adv 2011;1:012102.
[23] Weon BM, Lee JS, Je JH, Fezzaa K. X-ray-induced water vaporization. Phys Rev E 2011;84:032601.
[24] Weon BM, Kim JT, Je JH, Yi JM, Wang S, Lee WK. Colloid coalescence with focused x rays. Phys Rev Lett 2011;107:018301.
[25] Lee JS, Weon BM, Park SJ, Je JH, Fezzaa K, Lee WK. Size limits the formation of liquid jets during bubble bursting. Nat Commun 2011;2:367.
[26] Weon BM, Je JH. Coalescence preference depends on size inequality. Phys Rev Lett 2012;108:224501.
[27] Waigh TA, Rau C. X-ray and neutral imaging with colloids. Curr Opin Colloid Interface Sci 2012;17:13-22.
[28] Sakdinawat A, Attwood D. Nanoscale X-ray imaging. Nat Photonics 2010;4: 840-8.
[29] Scheel M, Seemann R, Brinkmann M, Di Michiel M, Sheppard A, Breidenbach B, Herminghaus S. Morphological clues to wet granular pile stability. Nat Mater 2008;7:189-93.
[30] Beerlink A, Mell M, Tolkiehn M, Salditt T. Hard x-ray phase contrast imaging of black lipid membranes. Appl Phys Lett 2009;95:203703.
[31] Hertz HM, Bertilson M, Hofsten OV, Gleber SC, Sedlmair J, Thieme J. Laboratory X-ray microscopy for high-resolution imaging of environmental colloid structure. Chem Geol 2011, http://dx.doi.org/10.1016/j.chemgeo.2011.07.012.
[32] Norby P. In-situ XRD, as a tool to understanding zeolite crystallization. Curr Opin Colloid Interface Sci 2006;11:118-25.
[33] Guttmann P, Bittencout C, Rehbein S, Umek P, Ke X, Tendeloo GV, Ewels CP, Schneider G. Nanoscale spectroscopy with polarized X-rays by NEXAFS-TXM. Nat Photonics 2011;6:25-8.
[34] Godard P, Carbone G, Allain M, Mastropietro F, Chen G, Capello L, Diaz A, Metzger TH, Stangl J, Chamard V. Three-dimensional high-resolution quantitative microscopy of extended crystals. Nat Commun 2011;2:568.
[35] Ice GE, Budai JD, Pang WL. The race to X-ray microbeam and nanobeam science. Science 2011;334:1234-9.
[36] Bevan MA, Eichmann SL. Optical microscopy measurements of kT-scale colloidal interactions. Curr Opin Colloid Interface Sci 2011;16:149-57.
[37] Lee SH, Roichman Y, Yi GR, Kim SH, Yang SM, van Blaaderen A, van Oostrum P, Grier DG. Characterizing and tracking single colloidal particles with video holographic microscopy. Opt Express 2007;15:18275-82.
[38] Kaz DA, McGorty R, Mani M, Brenner MP, Manoharan VN. Physical ageing of the contact line on colloidal particles at liquid interfaces. Nat Mater 2012;11: 138-42.
[39] Crocker JC, Grier DG. Methods of digital video microscopy for colloidal studies. J Colloid Interface Sci 1996;179:298-310.
[40] Murray CA, Grier DG. Video microscopy of monodisperse colloidal systems. Annu Rev Phys Chem 1996;47:421-62.
[41] Habdas P, Weeks ER. Video microscopy of colloidal suspensions and colloidal crystals. Curr Opin Colloid Interface Sci 2002;7:196-203.
[42] Prasad V, Semwogerere D, Weeks ER. Confocal microscopy of colloids. J Phys Condens Matter 2007;19:113102.
[43] Jenkins MC, Egelhaaf SU. Confocal microscopy of colloidal particles: towards reliable, optimum coordinates. Adv Colloid Interface Sci 2008;136:65-92.
[44] Besseling R, Isa L, Weeks ER, Poon WCK. Quantitative imaging of colloidal flows. Adv Colloid Interface Sci 2009;146:1–17.
[45] Rasa M, Kuipers BWM, Philipse AP. Atomic force microscopy and magnetic force microscopy study of model colloids. J Colloid Interface Sci 2002;250:303-15.
[46] Butt HJ, Berger R, Bonaccurso E, Chen Y, Wang J. Impact of atomic force microscopy on interface and colloid science. Adv Colloid Interface Sci 2007;133:91–104.
[47] Harth K, Schulz B, Bahr C, Stannarius R. Atomic force microscopy of menisci of free-standing smectic films. Soft Matter 2011;7:7103-11.
[48] Voitchovsky K, Kuna JJ, Contera SA, Tosatti E. Direct mapping of the solid–liquid adhesion energy with subnanometre resolution. Nat Nanotechnol 2010;5:401-5.
[49] Grogan JM, Rotkina L, Bau HH. In situ liquid-cell electron microscopy of colloid aggregation and growth dynamics. Phys Rev E 2011;83:061405.
[50] Isa L, Lucas F, Wepf R, Reimhult E. Measuring single-nanoparticle wetting properties by freeze-fracture shadow-casting cryo-scanning electron microscopy. Nat Commun 2011;2:438.
[51] Poon WCK, Weeks ER, Royall CP. On measuring colloidal volume fractions. Soft Matter 2012;8:21-30.
[52] Ortega F, Ritacco H, Rubio RG. Interfacial microrheology: particle tracking and related techniques. Curr Opin Colloid Interface Sci 2010;15:237-45.
[53] Stevens N, Ralston J, Sedev R. The uniform capillary model for packed beds and particle wettability. J Colloid Interface Sci 2009;337:162-9.
[54] Chao W, Harteneck BD, Liddle JA, Anderson EH, Attwood DT. Soft X-ray microscopy at a spatial resolution better than 15 nm. Nature 2005;435:1210-3.
[55] Huang X, Nelson J, Kirz J, Lima E, Marchesini S, Miao H, Neiman AM, Shapiro D, Steinbrener J, Stewart A, Turner JJ, Jacobsen C. Soft x-ray diffraction microscopy of a frozen hydrated yeast cell. Phys Rev Lett 2009;103:198101.
[56] Bertilson M, von Hofsten O, Vogt U, Holmberg A, Christakou AE, Hertz HM. Laboratory soft-x-ray microscope for crytomography of biological specimens. Opt Lett 2011;36:2728-30.
[57] Neuhäusler U. Soft x-ray spectromicroscopy on hydrated colloidal and environmental science samples [dissertation]. Göttingen (Germany): Georg-August-Universität; 1999.
[58] Grunwaldt JD, Schroer CG. Hard and soft X-ray microscopy and tomography in catalysis: bridging the different time and length scales. Chem Soc Rev 2010;39: 4741-53.
[59] Chao W, Fischer P, Tyliszczak T, Rekawa S, Anderson E, Naulleau P. Real space soft x-ray imaging at 10 nm spatial resolution. Opt Express 2012;20: 9777-83.
[60] Chen TY, Chen YT, Wang CL, Kempson IM, Lee WK, Chu YS, Hwu Y, Margaritondo G. Full-field microimaging with 8 keV X-rays achieves a spatial resolutions better than 20 nm. Opt Express 2011;19:19919-24.
[61] Sun Y. Watching nanoparticle kinetics in liquid. Mater Today 2012;15:140-7.
[62] Binks BP, Horozov TS. Colloidal particles at liquid interfaces. Cambridge: Cambridge Univ. Press; 2006.
[63] Ramsden W. Separation of solids in the surface-layers of solutions and 'suspensions' (observations on surface-membranes, bubbles, emulsions, and mechanical coagulation). Preliminary Account, 72. , Phil Trans R Soc Lond; 1903. p. 156-64.
[64] Pickering S. Emulsions. J Chem Soc 1907;91:2001-21.
[65] Dinsmore AD, Hsu MF, Nikolaides MG, Marquez M, Bausch AR, Weitz DA. Colloidosomes: selectively permeable capsules composed of colloidal particles. Science 2002;298:1006-9.
[66] Binks BP, Murakami R. Phase inversion of particle-stabilized materials from foams to dry water. Nat Mater 2006;5:865-9.
[67] Niu Z, He J, Russell TP, Wang Q. Synthesis of nano/microstructures at fluid interfaces. Angew Chem Int Ed 2010;49:10052-66.
[68] McGorty R, Fung J, Kaz D, Manoharan VN. Colloidal self-assembly at an interface. Mater Today 2010;13:34-42.
[69] Pieranski P. Two-dimensional interfacial colloidal crystals. Phys Rev Lett 1980;45:569-72.
[70] Zwanikken J, van Roij R. Charged colloidal particles and small mobile ions near the oil–water interface: destruction of colloidal double layer and ionic charge separation. Phys Rev Lett 2007;99:178301.
[71] Paunov VN. Novel method for determining the three-phase contact angle of colloid particles adsorbed at air–water and oil–water interfaces. Langmuir 2003;19:7970-6.
Arnaudov LN, Cayre OJ, Stuart MAC, Stoyanov SD, Paunov VN. Measuring the three-phase contact angle of nanoparticles at fluid interfaces. Phys Chem Chem Phys 2003;12:328-31.
[72] Zeng C, Bissig H, Dinsmore AD. Particles on droplets: from fundamental physics to novel materials. Solid State Commun 2006;139:547-56.
[73] Antl L, Goodwin JW, Hill RD, Ottewill RH, Owens SM, Papworth S, Waters JA. The preparation of poly(methyl methacrylate) latices in non-aqueous media. Colloids Surf 1986;17:67-78.
[74] Pusey PN, van Megen W. Phase behaviour of concentrated suspensions of nearly hard spheres. Nature 1986;320:340-2.
[75] Auer S, Poon WCK, Frenkel D. Phase behavior and crystallization kinetics of poly-12-hydroxystearic-coated polymethylmethacrylate colloids. Phys Rev E 2003;67:020401.
[76] Nikolaides MG. Colloids at Liquid-Liquid Interfaces. Ph. D. thesis, Technische Universitat Munchen; 2001.
[77] Fowkes FM. Determination of interfacial tensions, contact angles, and dispersion forces in surfaces by assuming additivity of intermolecular interactions in surfaces. J Phys Chem 1962;66:382.
Additivity of intermolecular forces at interfaces. I. Determination of the contribution to surface and interfacial tensions of dispersion forces in various liquids. J Phys Chem 1963;67:2538-41.
Attractive forces at interfaces. Ind Eng Chem 1962;56:40-52.
[78] Erbil HY. Surface chemistry of solid and liquid interfaces. Oxford: Blackwell; 2006.
[79] Schofield A. http://www.ph.ed.ac.uk/~abs/.
[80] Peng Y, Chen W, Fischer TM, Weitz DA, Tong P. Short-time self-diffusion of nearly hard spheres at an oil–water interface. J Fluid Mech 2009;618:243-61.
[81] Xu L, Davies S, Schofield AB, Weitz DA. Dynamics of drying in 3D porous media. Phys Rev Lett 2008;101:094502.
[82] Fujimatsu T, Fujita H, Hirota M, Okada O. Interfacial deformation between an impacting water drop and a silicone-oil surface. J Colloid Interface Sci 2003;264:212-20.
[83] Maestro A, Bonales LJ, Ritacco H, Rubio RG, Ortega F. Effect of the spreading solvent on the three-phase contact angle of microparticles attached at fluid interfaces. Phys Chem Chem Phys 2010;12:14115-20.
[84] Dokou E, Barteau MA, Wagner NJ, Lenhoff AM. Effect of gravity on colloidal deposition studied by atomic force microscopy. J Colloid Interface Sci 2001;240:9–16.
[85] Oettel M. Entrapment of charged, nonwetting colloids near oil–water interfaces. Phys Rev E 2007;76:041403.
[86] Kegel WK, Groenewold J. Scenario for equilibrium solid-stabilized emulsions. Phys Rev E 2009;80:030401.
[87] Dierolf M, Menzel A, Thibault P, Schneider P, Kewish CM, Wepf R, Bunk O, Pfeiffer F. Ptychographic X-ray computed tomography at the nanoscale. Nature 2010;467:436-9.
[88] Huotari S, Pylkkänen T, Verbeni R, Monaco G, Hämäläinen K. Direct tomography with chemical-bond contrast. Nat Mater 2011;10:489-93.
[89] Clark JN, Huang X, Harder R, Robinson IK. High-resolution three-dimensional partially coherent diffraction imaging. Nat Commun 2012;3:993.
[90] Zanette I, Bech M, Rack A, Le Duc G, Tafforeau P, David C, Mohr J, Pfeiffer F, Weitkamp T. Trimodal low-dose X-ray tomography. Proc Natl Acad Sci U S A 2012, http://dx.doi.org/10.1073/pnas.1117861109.
[91] Hunter GL, Weeks ER. The physics of the colloidal glass transition. Rep Prog Phys 2012;75:066501.

[92] Zaera F. Probing liquid/solid interfaces at the molecular level. Chem Rev 2012;112:2920-86.

[93] National Research Council (US) Committee on Revealing Chemistry through Advanced Chemical Imaging. Visualizing chemistry: the progress and promise of advanced chemical imaging. Washington, D.C.: National Academies Press; 2006

[94] Cheong FC, Krishnatreya BJ, Grier DG. Strategies for three-dimensional particle tracking with holographic video microscopy. Opt Express 2010;18: 13563-73.

[95] Fung J, Perry RW, Dimiduk TG, Manoharan VN. Imaging multiple colloidal particles by fitting electromagnetic scattering solutions to digital holograms. J Quant Spectrosc Radiat Transfer 2012, http://dx.doi.org/10.1016/j.jqsrt.2012.06.007.

[96] Klein S, Petersen S, Taylor U, Rath D, Barcikowski S. Quantitative visualization of colloidal and intracellular gold nanoparticles by confocal microscopy. J Biomed Opt 2010;15:036015.

[97] Muluneh M, Sprakel J, Wyss HM, Mattsson J, Weitz DA. Direct visualization of pH-dependent evolution of structure and dynamics in microgel suspensions. J Phys Condens Matter 2011;23:505101.

[98] Harke B, Ullal CK, Keller J, Hell SW. Three-dimensional nanoscopy of colloidal crystals. Nano Lett 2008;8:1309-13.

[99] Lauterbach MA, Ullal CK, Westphal V, Hell SW. Dynamic imaging of colloidal-crystal nanostructures at 200 frames per second. Langmuir 2010;26:14400-4.

[100] Hilhorst J, van Schooneveld MM, Wang J, de Smit E, Tyliszczak T, Raabe J, Hitchcock AP, Obst M, de Groot FMF, Petukhov AV. Three-dimensional structure and defects in colloidal photonic crystals revealed by tomographic scanning transmission X-ray microscopy. Langmuir 2012;28:3614-20.

[101] Geoghegan M, Krausch G. Wetting at polymer surfaces and interfaces. Prog Polym Sci 2003;28:261-302.

[102] Cherney DP, Harris JM. Confocal Raman microscopy of optical-trapped particles in liquids. Annu Rev Anal Chem 2010;3:277-97.